Johann Radon Institute for
Computational and Applied Mathematics
Austrian Academy of Sciences (ÖAW)

An efficient Reconstruction Method for Ground Layer Adaptive Optics with mixed Natural and Laser Guide Stars

R. Wagner, T. Helin, A. Obereder, R. Ramlau

RICAM-Report 2015-20

An efficient Reconstruction Method for Ground Layer Adaptive Optics with mixed Natural and Laser Guide Stars

Roland Wagner*†, Tapio Helin‡, Andreas Obereder*§and Ronny Ramlau*¶

September 23, 2015

Abstract

The imaging quality of modern ground based telescopes like the planned European Extremely Large Telescope is affected by atmospheric turbulence. In consequence, they heavily depend on stable and high-performance Adaptive Optics (AO) systems. Using measurements of incoming light from guide stars, an AO system compensates for the effects of turbulence by adjusting so-called deformable mirror(s) (DM) in real-time.

In this paper, we introduce a novel reconstruction method for the Ground Layer Adaptive Optics (GLAO). In the literature, a common approach to this problem is to use Bayesian inference in order to model the specific noise structure appearing due to spot elongation (see [5]). This approach leads to large coupled systems with high computational effort. Recently, fast solvers of linear order, i.e., with computational complexity $O(n)$, where n is the number of DM-actuators, have emerged [18]. However, the quality of such methods typically degrades in low flux conditions. Our key contribution is to achieve the high quality of the standard Bayesian approach while at the same time maintaining the linear order speed of the recent solvers. Our method is based on performing a separate preprocessing step before applying the cumulative reconstructor (CuReD, [27]).

The efficiency and performance of the new reconstructor are demonstrated using the OCTOPUS, the official end-to-end simulation enviroment of the ESO for extremely large telescopes [15]. For more specific simulations we also use the MOST toolbox [1].

1 Introduction

The image quality of modern ground based telescopes like the planned European Extremely Large Telescope (E-ELT) depends heavily on Adaptive Optics (AO) systems. AO systems use the measurements of incoming wavefronts from

*Johann Radon Institute for Computational and Applied Mathematics (RICAM), Altenbergerstrasse 69, 4020 Linz, Austria

†e-mail: roland.wagner@ricam.oeaw.ac.at

‡University of Helsinki, Gustaf Hallströmin katu 2b, FI-0014 Helsinki, Finland

§MathConsult GmbH, Altenbergerstrasse 69, 4040 Linz, Austria

¶Johannes Kepler University Linz, Altenbergerstrasse 69, 4040 Linz, Austria

reference sources (guide stars) for the reconstruction of the turbulence above the telescope. Based on the turbulence profile, the shape of deformable mirror(s) (DM) is determined such that the image of the scientific objects is corrected after reflection on the deformable mirror(s). Several AO systems are currently in use or proposed for ELTs, like Single Conjugate Adaptive Optics (SCAO), Ground Layer Adaptive Optics (GLAO), Multi Conjugate Adaptive Optics (MCAO) and Multi Object Adaptive Optics (MOAO). With the exception of SCAO, all systems rely on measurements from several guide stars, taken by a wavefront sensor for each guide star. However, as the coverage of the sky with sufficiently bright natural guide stars (NGS) is low, laser guide stars (LGS) are used. Unfortunately, LGS introduce additional effects into the modeling of the measured data, e.g., cone effect, tip/tilt indeterminacy and spot elongation, and hence affect the reconstruction of the atmosphere or the shape of the deformable mirror.

In this paper, we propose a new reconstruction method for Ground Layer Adaptive Optics. In GLAO, several guide stars, each associated to a wavefront sensor, and a single mirror is used for the correction of the turbulence in the layer closest to the ground, where usually most of the atmospheric turbulence is located. There are several approaches for the reconstruction of the optimal mirror shape for GLAO. The simplest one consists in averaging the measurements of the incoming wavefronts from the guide stars, reconstruct the wavefront from the averaged measurements and deform the mirror accordingly [18, 5]. Alternatively, the wavefronts can be reconstructed separately and then be averaged [18]. More evolved approaches consider a GLAO system as an MCAO system with one mirror, i.e., an atmospheric tomography and a good mirror fitting is needed. For the latter approach, any of the many suggested computational methods for MCAO can be used [12, 26, 25, 20, 21, 16, 24, 8, 7, 11, 10, 9].

GLAO systems use a combination of natural and laser guide stars. As mentioned above, spot elongation is a well-documented effect complicating the use of laser guide stars (LGS) on Extremely Large Telescopes (ELT). When an LGS is observed with a Shack–Hartmann wavefront sensor, the spot registered on each subaperture is elongated due to the parallax effect. The elongation degrades the measurement accuracy and the error increases linearly with the elongation of the spot in the direction of the centroid [5]. Furthermore, spot elongation introduces correlation between the X and Y measurements in the subaperture [23]. Correction for spot elongation is in particular needed for the planned generation of Extremely Large Telescopes.

In the Bayes approach it is natural to model the spot elongation as a specific noise distribution. There is a line of research [23, 3, 2, 5, 6] studying such an approach in different adaptive optics configurations. The standard approach is to consider the operator that maps the turbulent atmosphere to the Shack–Hartmann measurements, and include the noise distribution of the spot elongation directly into the reconstruction of the atmosphere, e.g., by the minimization of an appropriate Tikhonov functional, which takes the form

$$\min_{\varphi} \|\Gamma\varphi - s\|_{C_n} + \alpha\|s\|_{C_p},$$

or, equivalently, solving

$$\Gamma^\dagger C_n \Gamma \varphi = \Gamma^\dagger s,$$

where Γ is the (Shack-Hartmann) WFS-operator and $\Gamma^\dagger$ its pseudo inverse, φ the incoming wavefront, s the vector of all WFS measurements, C_n the covariance noise matrix and C_p the prior noise matrix. This approach leads to a large coupled system of linear equations for the atmospheric layers and thus causes a high computational effort.

Within this paper, we discuss the benefits of compensating for the spot elongation in a separate and fast preprocessing step. We formulate a denoising problem where the noise model from [5] is assumed. X and Y measurements on one subaperture of a given WFS are statistically dependent due to spot elongation. Our algorithm eliminates this dependence and thus decouples X and Y measurements of the LGS. Different subapertures on a given WFS and also different WFSs are statistically independent. Therefore, measurements for each laser guide star can be treated separately. We discuss in particular a numerical example of the correction for spot elongation for a SCAO system equipped with a laser guide star. The main body of our work is to demonstrate the advantage of our preprocessing approach for a GLAO system, when a modified cumulative reconstructor (CuReD) [27] is utilized.

Our whole proposed algorithm is potentially also applicable to Multi-Conjugate AO (MCAO), Laser Tomography AO (LTAO) and Multi-Object AO (MOAO) to correct for the ground layer of the atmosphere. The reconstructed ground layer can be used in tomographic reconstructors straight forward. In some cases the speed of a tomographic reconstructor might become slower due to the additional operations.

As our simulation environment we use two different toolboxes. Our main simulation enviroment is the OCTOPUS, the official end-to-end ELT simulation environment of the ESO [15]. This is used especially for the simulations regarding GLAO. For more specific tests regarding the statistics we used the MOST toolbox developed by our research group in Linz, Austria [1].

The paper is organized as follows. In Section 2 we describe some preliminaries to Bayesian inference in adaptive optics. Especially, we discuss the choice of prior and noise statistics. Our preprocessing step in introduced in Section 3 where we study its qualitative denoising effect (Section 3.2) and performance on a classical SCAO system. Our main results are represented in Section 4 where the impact of the preprocessing method is demonstrated in OCTOPUS using different imaging scenarios. Finally, we give some remarks and conclusions in Sections 5 and 6.

2 Bayesian inference in adaptive optics

2.1 Preliminaries

In Bayesian paradigm the reconstruction problem is cast into a question of statistical inference: what information do we have regarding the possible values

of the unknown? Consider the equation

$$\mathbf{S} = \mathbf{A}\mathbf{X} + \mathbf{E}, \tag{1}$$

where $\mathbf{S} \in \mathbb{R}^m$, $\mathbf{X} \in \mathbb{R}^n$ and $\mathbf{E} \in \mathbb{R}^m$ are the measured data, the unknown and the measurement noise, respectively. Moreover, the matrix $\mathbf{A} \in \mathbb{R}^{m\times n}$ models the physics behind the measurement.

The unknown quantities in (1) are in the Bayesian scheme replaced by random variables. The degree of information regarding their values is encoded into the corresponding probability distributions. A common choice in adaptive optics is to model both the prior and noise distributions, i.e., $\mathbf{X}$ and $\mathbf{E}$ using Gaussian statistics. We motivate this choice in more detail below. For now assume that $\mathbf{X} \sim \mathcal{N}(\mathbf{x}_0, \mathbf{\Sigma})$ and $\mathbf{E} \sim \mathcal{N}(\mathbf{e}_0, \mathbf{\Lambda})$ with positive definite covariance matrices $\mathbf{\Sigma} \in \mathbb{R}^{n\times n}$ and $\mathbf{\Lambda} \in \mathbb{R}^{m\times m}$.

Using the Bayes formula (cf., e.g., [13, Theorem 3.7]) for the problem above yields that the posterior distribution, i.e., $\mathbf{X}$ conditioned on a measurement $\mathbf{S} = \mathbf{s}$, is also Gaussian. In fact, the posterior mean is given by

$$\bar{\mathbf{x}} = (\mathbf{A}^T\mathbf{\Lambda}^{-1}\mathbf{A} + \mathbf{\Sigma}^{-1})^{-1}(\mathbf{A}^T\mathbf{\Lambda}^{-1}(\mathbf{s} - \mathbf{e}_0) + \mathbf{\Sigma}^{-1}\mathbf{x}_0).$$

In what follows, the structure of the covariance are fixed up to a constant, i.e., $\mathbf{\Sigma} = \sigma^2_{prior}\widetilde{\mathbf{\Sigma}}$ and $\mathbf{\Lambda} = \sigma^2_{noise}\widetilde{\mathbf{\Lambda}}$ where the variances σ^2_{prior} and σ^2_{noise} are case-dependent. An equivalent way to recover the posterior mean is then to find the minimizer

$$\bar{\mathbf{x}} = \operatorname*{argmin}_x \left(\|\widetilde{\mathbf{\Lambda}}^{-1/2}(\mathbf{A}\mathbf{x} - \mathbf{s}_0 + \mathbf{e}_0)\|_2^2 + \frac{\sigma^2_{noise}}{\sigma^2_{prior}}\|\widetilde{\mathbf{\Sigma}}^{-1/2}(\mathbf{x} - \mathbf{x}_0)\|_2^2 \right).$$

In this paper we concentrate in studying the properties of the posterior mean. The optimization of parameter $\alpha = \frac{\sigma^2_{noise}}{\sigma^2_{prior}}$ plays a key role in the reconstruction process. In the following sections the noise and prior models are introduced and motivated in detail.

2.2 Statistical modelling of noise and prior

Noise statistics produced by LGS with spot elongation

Let us describe the noise model for spot elongation introduced in [5]. The elongation of the SH-WFS spot at a given subaperture can be approximated by a vector (cf. [23])

$$\boldsymbol{\beta} = \frac{\mathrm{FWHM}_{Na}}{h_0^2}(\mathbf{x} - \mathbf{x}_{LLT}), \tag{2}$$

where vectors $\mathbf{x}$ and $\mathbf{x}_{LLT}$ describe the corresponding coordinates of the center of the subaperture and the laser launch telescope (LLT) in the pupil plane in meters, respectively. Moreover, h_0 is the central altitude in meters and FWHM_{Na} is the Gaussian vertical density profile of full width at half maximum of the sodium layer in the atmosphere in meters. Thus, $\boldsymbol{\beta}$ and the following derived quantities are dimensionless. The normalized elongated and non-elongated directions for the subaperture are denoted by

$$\mathbf{e} = \frac{\boldsymbol{\beta}}{\|\boldsymbol{\beta}\|} \quad \text{and} \quad \mathbf{n} = \frac{(-(\beta)_2, (\beta)_1)^T}{\|\boldsymbol{\beta}\|}. \tag{3}$$

In the following we consider a simplified imaging situation with G SH-WFSs each composed of N subapertures. For convenience each WFS observes a laser guide star. We highlight the index of the subaperture and the WFS by using notation $\boldsymbol{\beta}_n^g$, $\mathbf{e}_n^g$ and $\mathbf{n}_n^g$ for $n = 1, ..., N$ and $g = 1, ..., G$.
In the literature the noise observed in the subaperture with indices g and n is assumed to have a Gaussian distribution with zero expectation and covariance

$$\begin{aligned} \mathbf{C}_{g,n} &= \sigma_{noise}^2 \cdot \mathbf{n}_n^g (\mathbf{n}_n^g)^T + \sigma_{noise}^2 \left(1 + \frac{\|\boldsymbol{\beta}\|^2}{\theta^2}\right) \cdot (\mathbf{e}_n^g)(\mathbf{e}_n^g)^T \\ &= \sigma_{noise}^2 \begin{pmatrix} 1 + \frac{(\beta_n^g)_1^2}{\theta^2} & \frac{(\beta_n^g)_1 (\beta_n^g)_2}{\theta^2} \\ \frac{(\beta_n^g)_1 (\beta_n^g)_2}{\theta^2} & 1 + \frac{(\beta_n^g)_2^2}{\theta^2} \end{pmatrix}, \end{aligned} \tag{4}$$

where σ_{noise} stands for the noise variance of a non-elongated measurement and θ is the FWHM of the non-elongated spot. It is natural to assume that the noise in two separate subapertures is generated by independent random variables. Consequently, the noise model for the full measurement vector inherits a Gaussian distribution with zero expectation and a block diagonal covariance matrix

$$\mathbf{C}_{noise} = \mathrm{diag}(\mathbf{C}_{1,1}, \ldots, \mathbf{C}_{1,N}, \mathbf{C}_{2,1}, \ldots, \mathbf{C}_{G,N}). \tag{5}$$

We point out that the centroiding algorithm can already mitigate the elongation. In our simulations, centroiding is done by center of gravity algorithm incorporated in Octopus. In this case an approximate elongation vector and hence also a covariance have to be tuned numerically. The effect of the centroiding algorithm in OCTOPUS has been considered in [5]. We leave these considerations regarding our preprocessing step for future studies.

Empirical estimation of the prior

The statistical distributions of measurements and turbulence have a direct connection via the imaging geometry. In open-loop setting it would be rather straightforward to estimate a reliable prior model for the measurements based on classical turbulence models. However, the problem is more complicated in the closed-loop setting, since the residual measurements are naturally affected by the reconstruction procedure.

Due to the severe time constraints in adaptive optics we take a simplified approach by assuming that the measurement statistics is stationary also in closed-loop. Moreover, our key assumption is that measurements on each subaperture are identically distributed and jointly independent. In order to support the second claim we simulated an SCAO system on MOST described in Table 1 where we assumed an extreme high-flux setting (roughly no noise) and used CuReD for reconstruction.

We simulated a large set of measurements $\{\mathbf{s}_t\}_{t=1}^T$ for $T = 5000$ and computed the empirical mean $\mathbf{m}_T \in \mathbb{R}^{84^2}$ and covariance matrix $\mathbf{C}_T \in \mathbb{R}^{84^2 \times 84^2}$. In particular, we sampled only every tenth screen to achieve lower statistical dependence in time. Further, only the measurements from the active subapertures were sampled. We found that the results were similar for different atmosphere profiles and, consequently, restrict here to the results obtained with the ESO Standard atmosphere from [14]. Notice that the Shack–Hartmann mesurements

Table 1: **Description of the simulated SCAO system**

Telescope diameter	42 m
central obstruction	11.76 m
1 LGS Shack-Hartmann WFS	84×84 subapertures
wavelength λ	0.589 μm
WFS integration time	2 ms
Laser Launch Telescope	[0 ; 23]m
Na-layer altitude	90000 m
Na-layer FWHM	11400 m
1 DM at height 0 m	closed loop
DM actuator spacing	0.5 m

are dimensionless quantities that are linearly dependent on the wavelength (see Table 1).

It was clearly visible in our results that the empirical mean is zero to a good approximation: the ℓ_1-norm of m_T was of order 10^{-5} in all tests, giving an absolute value of the mean for the measurement on one subaperture of order 10^{-9}. We studied the empirical covariance $\mathbf{C}_T$ by decomposing it into diagonal and residual components, i.e., $\mathbf{C_T} = \mathbf{D_T} + \mathbf{E_T}$, where $\mathbf{D_T} = \mathrm{diag}(\mathbf{C}_T)$. We also found that the diagonal $\mathbf{D}_T$ is dominating: the respective ℓ^2-norms were $\|\mathbf{D}_T\|_{\ell^2} \approx 10^{-10}$ and $\|\mathbf{E}_T\|_{\ell^2} \approx 10^{-9}$. Considering that in this example there were 5044 active subapertures, the mean absolute values of entries of $\mathbf{D}_T$ and $\mathbf{E}_T$ are of the order 10^{-12} and 10^{-13}, respectively. Recall that while the measurements are linearly dependent on the wavelength λ, the variance depends on λ^2. Also, the values of $\mathbf{D}_T$ (illustrated in Figure 1) are of same order with a mean $\bar{\sigma}^2_{prior} = 6.24 * 10^{-12} = 18\lambda^2$. Thus it turns out in computations that couplings are introduced, e.g., by the DM correction, but those couplings are weak. As Bayesian inverse problems are known to be stable in the sense that small perturbation in the (Gaussian) prior introduces only a small perturbation in the posterior (cf., e.g., [22]) and, in consequence, the prior covariance can be modelled by a diagonal matrix to a good approximation.

We remark that if the WFSs (LGS and NGS) are sensing at the same wavelength, the prior covariance and the noise variance σ_{noise} in equation (4) scale identically with respect to the wavelength. In the following our reconstruction method requires estimating $\alpha = \sigma^2_{noise}/\bar{\sigma}^2_{prior}$. In consequence, working at a constant wavelength implies that α does not depend on the wavelength. All GS give full measurements.

Notice carefully that for the statistical inference method proposed below a choice of $\alpha > 0$ will lead to different statistics than obtained above for the residual measurements. That being said, our numerical simulations indicate that the crucial assumptions, zero-mean, independent and identically residual data, remain valid. Hence in what follows the choice of α is part of the optimization process for our method.

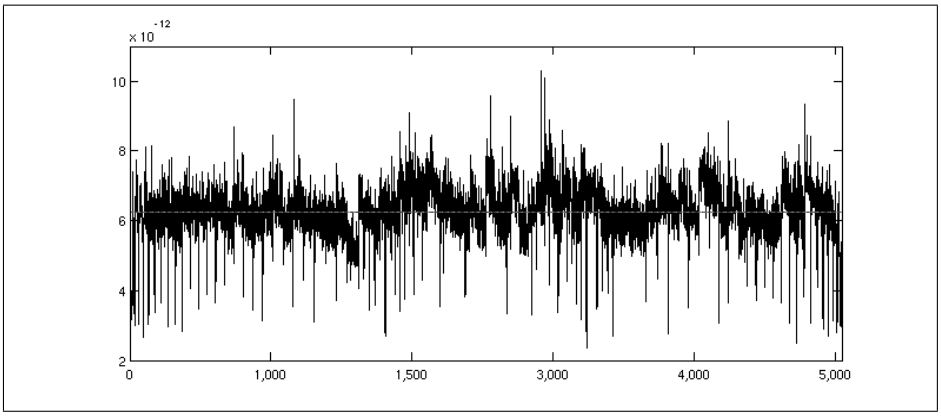

Figure 1: Diagonal values of the empirical covariance matrix. The y-axis represents the value of empirical variance at each subaperture indexed at the x-axis. The horizontal line stands for the mean of the diagonal values.

3 Bayesian approach to measurement denoising

3.1 A statistical denoising procedure

Consider the problem of denoising the measurement vector from the Bayesian perspective. Let us assume that the statistics of residual measurement is Gaussian with zero-mean and a covariance matrix $\mathbf{C}_{prior} = \frac{1}{\alpha}\mathbf{I}$. Clearly, the maximum a posteriori estimate solves the minimization problem

$$\mathbf{S}_{MAP} = \underset{\tilde{\mathbf{S}}}{\operatorname{argmin}} \|\mathbf{C}_{noise}^{-1/2}(\tilde{\mathbf{S}} - \mathbf{S}^{\delta})\|_2^2 + \alpha\|\tilde{\mathbf{S}}\|_2^2. \tag{6}$$

Since $\mathbf{C}_{noise}$ is block-diagonal and the prior covariance is diagonal, the problem above reduces to independent minimization problems at each subaperture. In conclusion, we notice that

$$(\mathbf{S}_{MAP})_{g,n} = \underset{\mathbf{S}\in\mathbb{R}^2}{\operatorname{argmin}} \| \left(\mathbf{C}_{g,n}\right)^{-1/2} \left(\mathbf{S} - \mathbf{S}_{g,n}^{\delta}\right) \|_2^2 + \alpha\|\mathbf{S}\|_2^2, \tag{7}$$

and, consequently,

$$(\mathbf{S}_{MAP})_{g,n} = (\mathbf{I} + \alpha\mathbf{C}_{g,n})^{-1}\mathbf{S}_{g,n}^{\delta}. \tag{8}$$

The matrix on the right-hand side can be computed explicitly from the eigenvalue decomposition in equation (4). Namely, we have

$$\begin{aligned}(\mathbf{I} + \alpha\mathbf{C}_{g,n})^{-1} \quad &= \quad \frac{1}{1 + \alpha\sigma_{noise}^2} \cdot \mathbf{n}_n^g(\mathbf{n}_n^g)^T \\ &\quad + \frac{1}{1 + \alpha\sigma_{noise}^2(1 + \frac{\|\boldsymbol{\beta}_n^g\|^2}{\theta^2})} \cdot \mathbf{e}_n^g(\mathbf{e}_n^g)^T. \end{aligned} \tag{9}$$

Thus, the data preprocessing step has linear complexity and can be incorporated in an efficient way.

3.2 On the qualitative influence of preprocessing

In this Section we want to illustrate the effect of the preprocessing step to the noisy wavefront measurements. Hence we assume that the 'true' noise free measurements, i.e., without spot elongation are at our disposal. Our aim is to demonstrate that the preprocessing step reduces the noise in the measurements already in the case with one single LGS. We demonstrate the impact using a

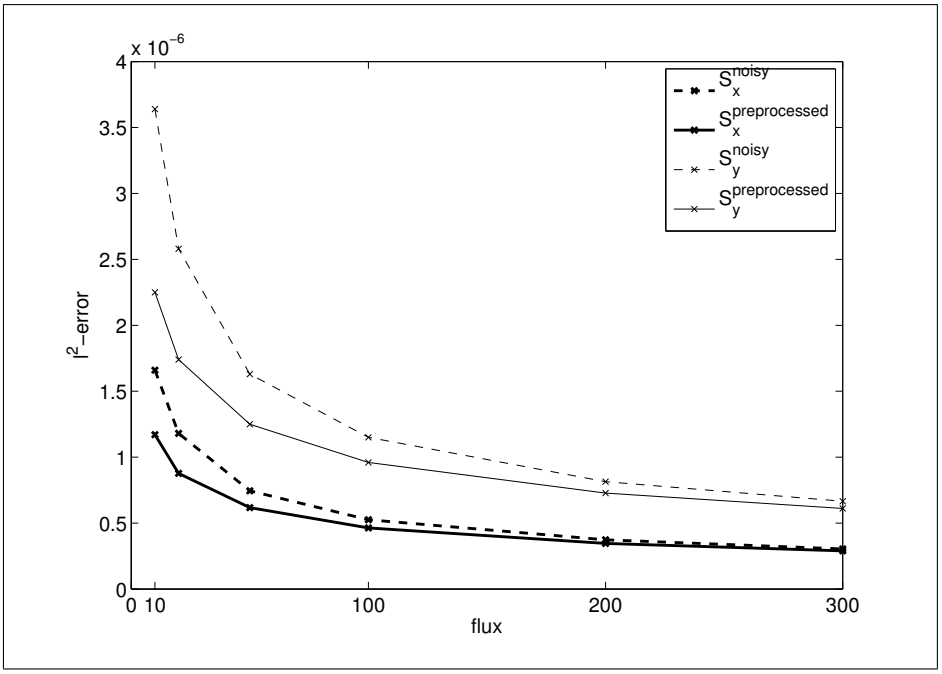

Figure 2: Effect of the preprocessing on the ℓ^2-error of the measurements to the noise free measurements, where the ℓ^2-error is the square root of the sum of squared differences in the sample points.

telescope with 42 m diameter with the setting described in Table 1. However, note that the effect depends on the laser launch position of the telescope. We leave this aspect for future considerations as the SCAO system is not our focus in this work. The system was set up and simulated in MOST. For this problem, note that $\alpha = 0$ implies no preprocessing.

In our simulations we study different flux levels from 10 to 300 photons per subaperture per frame (see Figure 2). In the plot all used photon flux levels are indicated with crosses. Using different flux levels is of interest as a lower photon flux also leads to a lower signal to noise ratio. The numbers are time averages over the respective values from a simulation of 200 timesteps. One should note that MOST is not an end-to-end simulation tool like ESO's Octopus and thus tends to underestimate the effects of the atmosphere as in related OCTOPUS tests. This is the main reason why we use a lower photon flux as in the Ocotpus tests.

Depending on the flux of the LGS, the error in the ℓ^2-norm can be reduced

by 10 to 30 %, i.e., for the x-measurement the quantity

$$\frac{\|\mathbf{S}_x - \mathbf{S}_x^{preprocessed}\|_{\ell^2}}{\|\mathbf{S}_x - \mathbf{S}_x^{noisy}\|_{\ell^2}},$$

ranges between 0.7 and 0.9, where $\mathbf{S}_x$ are measurements coming from the simulated atmosphere without any read-out and measurement noise, $\mathbf{S}_x^{noisy}$ are measurements containing simulated noise such as spot elongation and read-out noise and $\mathbf{S}_x^{preprocessed}$ are the preprocessed measurements resulting from our denoising procedure. The improvement is higher for lower flux as there the signal to noise ratio is worse and thus elongation effects and noise have more influence on the quality of the measurements.

We conclude that the preprocessing has a positive effect already in case of just one LGS, which suggests an extension of the method towards more LGS or an combination between LGS and NGS.

3.2.1 Performance on an SCAO system

As demonstrated above the preprocessing step reduces the measurement noise produced by spot elongation and other sources and, in consequence, should also improve the quality of the wavefront reconstruction. To illustrate the impact of preprocessing to wavefront reconstruction, we simulated an LGS SCAO system as described in Table 1. The system was setup in Octopus. Different photon fluxes are simulated, varying between 20 and 500 photons per subaperture per frame. Our numerical simulations show that in closed loop the reconstruction quality in terms of Strehl Ratio increases by about two to five percent points. In extreme low flux settings the advantage is even more, as shown in Figure 3. The main benefit however is that the preprocessing step stabilizes the wavefront reconstruction and thus a higher integrator loop gain can be chosen, obtaining the same or even higher Strehl Ratios.

Note, that the analysis of the effects of spot elongation for the regularization does not take the tip tilt indeterminacy into account, thus further studies might be necessary.

4 Measurement preprocessing for GLAO

4.1 Principle concept for GLAO preprocessing

In this section we discuss the preprocessing scheme in the context of ground layer adaptive optics. It is well-known that a large amount of atmospheric turbulences is located close to the ground. By providing a good correction for the ground layer, the imaging quality would increase significantly over the full field of view. GLAO systems have been designed for this purpose. The idea in GLAO is to utilize several guide stars in order to achieve a high-resolution reconstruction of the ground layer. A typical GLAO system is designed with one deformable mirror.

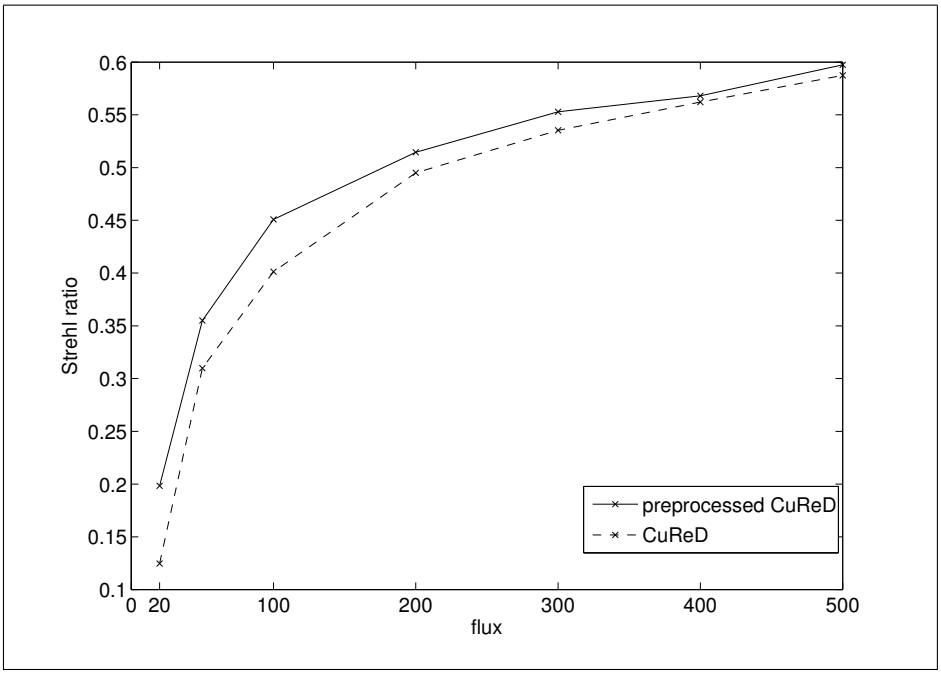

Figure 3: Effect of the preprocessing on the Strehl Ratio in an LGS SCAO System.

In literature, the reconstruction problem in GLAO is often approached using Bayesian inference and by postulating the data-to-reconstruction solver as a one-step method. As noted in the introduction, this leads to coupled systems and causes high computational effort. Our idea is to propose a preprocessing step for the measurements which removes most of the unwanted noise. In the second step we are able to apply a standard wavefront reconstructor to the denoised measurement vector. In our simulations we use a method called the Cumulative Reconstructor with domain decomposition (CuReD), which is a fast, matrix free wavefront reconstructor developed in [27, 17, 19]. Our approach leads to significant reductions in the computational effort, while providing a comparable quality for the reconstructions.

The preprocessing step proposed here could be seen as a simple weighted sum of the measurements - the weights being determined by the prior and noise statistics discussed in Section 2. We point out that a reversed method was used in [18], where the authors first reconstructed the incoming wavefronts front the measurements and afterwards applied weighting. However, the noise covariances of the reconstructed wavefronts is not sparse and produces again computational costs.

We recognize that by reconstructing only the ground layer one neglects the separation of the guide stars. However, this approximation is motivated by two properties: first, the separation of field of view between two WFSs is small even at the highest altitudes. In our examples, the separation of the centers (see

Figure 4) is at maximum 10 arcmin for two GS lying opposite to each other as the LGS are on a ring with 7.5 arcmin diameter and the NGS one third further outside. Secondly, most of the turbulence is located close to the ground.

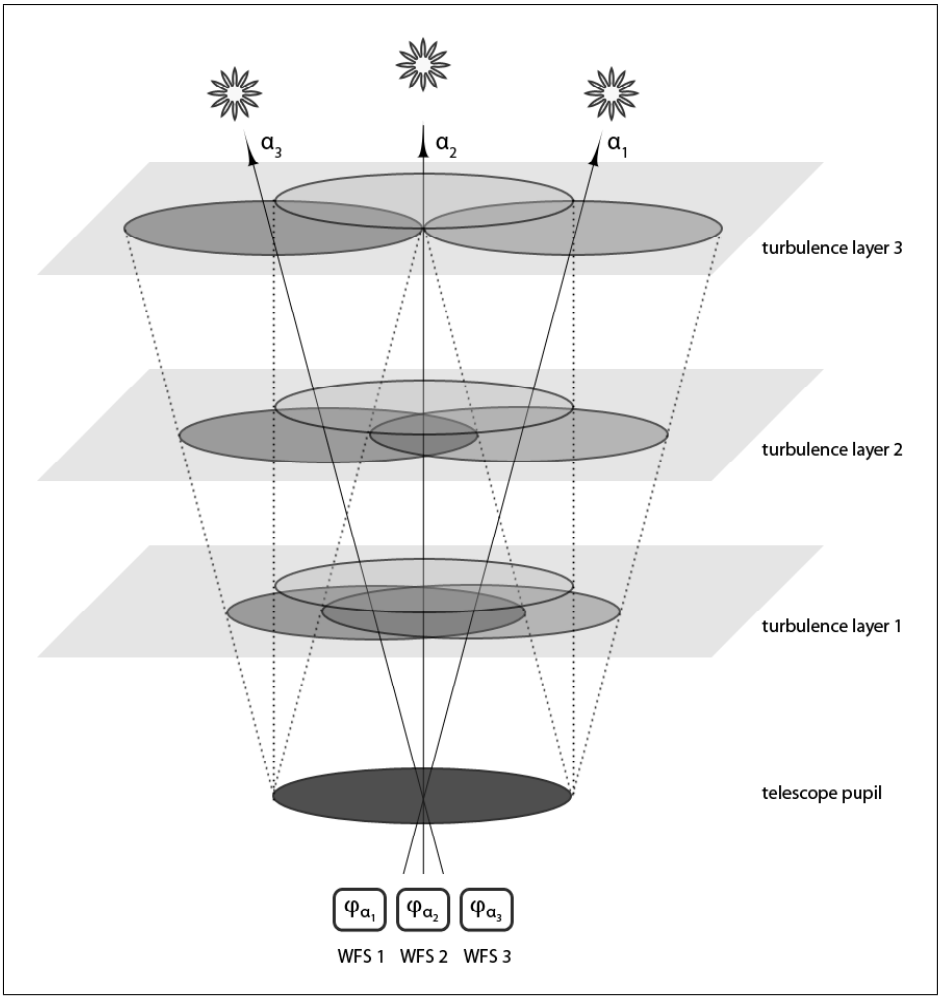

Figure 4: Scheme with three atmospheric layers and three WFS and GS.

4.2 Regularization by combining all WFS mesaurements

In GLAO we are given a set of measurements $\mathbf{S}^{\delta}_{g,n} \in \mathbb{R}^2$ at each subaperture $n = 1, ..., N$ for all guide stars indexed by g. The goal of our approach is to filter out the noise from spot elongation from the measurements by using a Bayesian approach. To this end the measurements are decomposed into a part representing the measurements coming from the real wavefront without any kind of noise and another part representing the noise. The first part should be the same for all WFS as they all sense the same atmosphere. S_n are the measurements from the real wavefront, δ_n are the measurement noise and S^{δ}_n are the measurements.

Below, for each subaperture n we explicitly solve Bayes-optimal measurements $\mathbf{S}_n \in \mathbb{R}^2$ of the ground-layer given such measurements. Let us combine the measurements $\mathbf{S}^\delta_{g,n}$, $g = 1, ..., G$ into a system

$$\mathbf{S}^\delta_n = \tilde{\mathbf{I}}\mathbf{S}_n + \boldsymbol{\delta}_n,$$

where

$$\mathbf{S}^\delta_n = \begin{pmatrix} \mathbf{S}^\delta_{1,n} \\ \vdots \\ \mathbf{S}^\delta_{G,n} \end{pmatrix} \in \mathbb{R}^{2G}, \quad \boldsymbol{\delta}_n = \begin{pmatrix} \boldsymbol{\delta}_{1,n} \\ \vdots \\ \boldsymbol{\delta}_{G,n} \end{pmatrix} \in \mathbb{R}^{2G},$$

and $\tilde{\mathbf{I}} = (\mathbf{I}_{2\times 2} \otimes ... \otimes \mathbf{I}_{2\times 2})^\top \in \mathbb{R}^{2\times 2G}$. The noise covariance is now given by $\mathbf{C}_n = \mathrm{diag}(\mathbf{C}_{1,n}, \ldots, \mathbf{C}_{G,n})$. Following Section 2 we find that the maximum a posteriori estimate on each subaperture n satisfies

$$\begin{aligned} \mathbf{S}_n &= (\tilde{\mathbf{I}}^T \mathbf{C}_n^{-1} \tilde{\mathbf{I}} + \alpha \mathbf{I})^{-1} \tilde{\mathbf{I}}^T \mathbf{C}_n^{-1} \mathbf{S}^\delta_n \\ &= \left(\sum_{g=1}^{G} \mathbf{C}^{-1}_{g,n} + \alpha \mathbf{I} \right)^{-1} \left(\sum_{g=1}^{G} \mathbf{C}^{-1}_{g,n} \mathbf{S}^\delta_{g,n} \right), \end{aligned}$$

where $\alpha = \sigma^2_{noise}/\bar{\sigma}^2_{prior}$. Equivalently, we obtain S_n by minimization

$$\mathbf{S}_n = \underset{\mathbf{S}\in\mathbb{R}^2}{\mathrm{argmin}} \sum_{g=1}^{G} \|\mathbf{S}^\delta_{g,n} - \mathbf{S}\|^2_{\mathbf{C}_n^{-1/2}} + \alpha \|\mathbf{S}\|_2^2.$$

Writing the MAP estimate in vector form $\mathbf{S}_n = (S_{n,x}, S_{n,y})^\top$ leads to

$$\begin{aligned} \begin{pmatrix} S_{n,x} \\ S_{n,y} \end{pmatrix} \quad = \quad & \frac{1}{\det \mathbf{C}_n} \begin{pmatrix} \alpha + \sum\limits_{g=1}^{G} \tau^{g,n}_{yy} & -\sum\limits_{g=1}^{G} \tau^{g,n}_{xy} \\ -\sum\limits_{g=1}^{G} \tau^{g,n}_{xy} & \alpha + \sum\limits_{g=1}^{G} \tau^{g,n}_{xx} \end{pmatrix} \\ & \times \begin{pmatrix} \sum\limits_{g=1}^{G} \tau^{g,n}_{xx} S^\delta_{g,n,x} + \tau^{g,n}_{xy} S^\delta_{g,n,y} \\ \sum\limits_{g=1}^{G} \tau^{g,n}_{xy} S^\delta_{g,n,x} + \tau^{g,n}_{yy} S^\delta_{g,n,y} \end{pmatrix}, \end{aligned}$$

where

$$\det \mathbf{C}_n = \left(\alpha + \sum_{g=1}^{G} \tau^{g,n}_{xx} \right) \left(\alpha + \sum_{g=1}^{G} \tau^{g,n}_{yy} \right) - \left(\sum_{g=1}^{G} \tau^{g,n}_{xy} \right)^2,$$

and

$$\mathbf{C}^{-1}_{g,n} = \begin{pmatrix} \tau^{g,n}_{xx} & \tau^{g,n}_{xy} \\ \tau^{g,n}_{xy} & \tau^{g,n}_{yy} \end{pmatrix}, \tag{10}$$

for any $n = 1, ..., N$ and $g = 1, ..., G$.

4.2.1 Taking NGS into account

Including the NGS measurements to the method is straightforward. For NGS the noise covariance is diagonal, since no spot elongation occurs. In this case only the low photon flux and read out noise contribute to the noise.

Suppose our GLAO system has G_L LGSs and G_N NGSs so that $G = G_L + G_N$. Also, let us also associate the first indeces to the LGSs. In this case, the formula for the mixed setting has the form

$$\begin{pmatrix} S_{n,x} \\ S_{n,y} \end{pmatrix} = \frac{1}{\det \mathbf{C}_n} \begin{pmatrix} \alpha + \sum_{g=1}^{G} \tau_{yy}^{g,n} & -\sum_{g=1}^{G_L} \tau_{xy}^{g,n} \\ -\sum_{g=1}^{G_L} \tau_{xy}^{g,n} & \alpha + \sum_{g=1}^{G} \tau_{xx}^{g,n} \end{pmatrix} \times \begin{pmatrix} \sum_{g=1}^{G} \tau_{xx}^{g,n} S_{g,n,x}^{\delta} + \tau_{xy}^{g,n} S_{g,n,y}^{\delta} \\ \sum_{g=1}^{G} \tau_{xy}^{g,n} S_{g,n,x}^{\delta} + \tau_{yy}^{g,n} S_{g,n,y}^{\delta} \end{pmatrix}, \tag{11}$$

where $\det \mathbf{C}_n = \left(\alpha + \sum_{g=1}^{G} \tau_{xx}^{g,n}\right)\left(\alpha + \sum_{g=1}^{G} \tau_{yy}^{g,n}\right) - \left(\sum_{g=1}^{G_L} \tau_{xy}^{g,n}\right)^2$ and τ_{kl}^{g} as before from (10). Notice that $\tau_{xy}^{g} = 0$ for $g = G_L + 1, ..., G$, i.e., corresponding to an NGS WFS.

4.2.2 Computational complexity

Let us analyze the preprocessing step described above in terms of computational complexity. First computational task is to set up the covariance matrices for all WFS. This can be done in a precomputing step and requires a memory of $4 * N * G$, where N is the number of active subapertures and G is the number of WFSs.

The computation of the weighted measurements requires to multiply the measurements with the covariances and summing up over all WFS. This leads to $(4 * G_L + 2 * G_N)$ operations for each line in the vector on the right hand side of (11). These two lines can be calculated independently for each of the N subapertures. Next, the scaling by means of the summed covariance matrices has to be applied, i.e., the matrix of (11), which requires another 4 calculations per line and subaperture.

Therefore all together $4 * (G_L + 1) + 2 * G_N$ operations per subaperture and per measurement type are required, i.e., in total $4 * (2 * (G_L + 1) + G_N) * N$ operations, and the calculations on each subaperture are independent. Note that using parallelization this number can be reduced as the calculations for the right-hand side vector in (11) are independent as well as the application of the matrix in front of it and furthermore each subaperture can be treated without taking any other into account. Finally, the CuReD reconstructs a wavefront from Shack-Hartmann measurements in $20N$ operations, where N is the number of active subapertures [19].

4.3 Octopus test results for a GLAO system

4.3.1 Simulated GLAO system

The simulations regarding the GLAO system (see Table 2) were fully performed on the Octopus simulation tool. Our settings included a 42 m mirror having wavefront sensors with 84×84 subapertures and one deformable mirror with 85×85 actuators. Altogether, nine WFSs were simulated. Six LGSs were set at a radius of 3.75 arcmin and three NGSs at one third further outside. The NGS WFS have 6×6 pixels/subaperture, LGS WFS have 20×20 pixels/subaperture and both are Shack-Hartmann WFS. The laser launch positions for the LGS are in the corners outside the telescope at a radius of 23 m from the telescope center. In all our simulations, the NGS photon flux is fixed to 500 photons/subaperture/frame and the LGS photon flux is varying from 20 to 500 photons/subaperture/frame. The read out noise is 3 electrons/pixel for both NGS and LGS. Tip-tilt is removed automatically from the LGS measurements.

As the model for the atmosphere, we chose the ESO standard atmosphere with 9 layers from [14]. The sodium layer is simulated with a central height $h_0 = 90\ km$ and with a Gaussian vertical density profile of full width at half maximum $\text{FWHM}_{Na} = 11.4\ km$.

The quality is measured by the 50% ensquared energy (EE) of the point spread function (PSF) in K band for the on-axis point after 500 iterations. The units are arcseconds. For the uncorrected atmosphere, the 50% EE in K band is 0.441 arcsec.

Referring to computational complexity from Section 4.2.2, for this setting $68N$ operations are required for the weighting procedure and another $20N$ for reconstructing the wavefront, where N is the number of active subapertures. The time for the weighting procedure can be reduced by pipelining and parallelizing the computation as each subaperture can be handled independently and almost all steps can be done independently for x- and y-measurements.

4.3.2 Results

In this section, the simulation results for our new approach to solve elongation problems in a GLAO system are compared to the ones obtained in [4] and in [18], using CuReD. We want to remark that for high flux LGS with and without spot elongation no preprocessing is needed, cf., e.g., [18]. Therefore, we focus on low flux imaging cases with spot elongation.

Recall from Section 2 that the parameter α needs to be tuned for each flux setting. In this process, one is in fact estimating the prior variance, since recall that $\alpha = \sigma^2_{noise}/\sigma^2_{prior}$ where it is known that $\sigma_{noise} \approx \frac{1}{N_{photons}}$, where $N_{photons}$ is the number of incoming photons/subaperture/frame. All other scaling effects will only change α slightly, but as the whole preprocessing step is rather stable there are no big changes. Due to limited resolution of WFSs and rather high NGS flux (500 photons/subaperture/frame), the mathematical problem is not very ill-posed. This is indicated by the method not being highly sensitive to

Table 2: **Description of the simulated GLAO system**

telescope diameter	42 m	
central obstruction	11.76 m	
Na-layer altitude	90000 m	
Na-layer FWHM	11400 m	
WFS integration time	2 ms	
1 DM at height 0 m	closed loop	
DM actuator spacing	0.5 m	
Guidestars	LGS	NGS
Shack-Hartmann WFS	6	3
subapertures per WFS	84×84	84×84
FoV	20 arcsec	2.4 arcsec
pixels per subaperture	20	6
wavelength λ	0.589 μm	0.5 μm
spot elongation	ON	–
spot FWHM	1.1"	–
detector read noise	3e/pixel/frame	3e/pixel/frame
separation angle wrt zenith	3.75 arcmin	5 arcmin

the prior variance. In fact, satisfactory results can be achieved even by setting $\alpha = 0$. However, the optimal value of α is typically of order 0.5.

It turned out that the entries of the noise covariance matrices have to be weighted for NGS and LGS, thus the entries in the NGS covariance matrices are only 6/20 of the original model. This is due to the different number of pixels per subaperture on the CCD for NGS and LGS, which reflects exactly this ratio, as these number influences the prior and the noise covariance. The results are presented in Figure 5, where we compare our method to ESO-MVM [4] and heuristically weighted CuReD [18]. In comparison to the heuristical weighting in [18], we obtain always better quality at the same speed of reconstruction. In contrast to the original CuReD approach, our approach can be used with higher integrator loop gain, around 0.7 to 0.9 compared to former 0.3 to 0.5. Regarding the MVM method in [4], our method reaches comparable quality in the high flux regime but surprisingly also in the extreme low flux setting. The advantages in speed are remarkable.

The result for 20 photons/subaperture/frame is 50% EE of the PSF within 0.2807 arcsec, so slightly better than 0.2809 arcsec from ESO-MVM and also better than 0.2864 arcsec from [18]. For 50 to 400 our results are a bit worse than the ones from [4], but the difference stays always smaller than 0.009 arcsec and our results are always better than those from [18]. In the highest flux case, 500 photons/subaperture/frame, our result is 0.2503 arcsec and so again close to ESO-MVM beeing 0.2492 arcsec, while in [18] only 0.2598 arcsec were obtained, when not changing the weighting between NGS and LGS, and even with changes nothing better than 0.2529 could be obtained. The best results were obtained with integrator loop gain 0.7 for 20 photons/subaperture/frame and with 0.9 for 500 photons/subaperture/frame. The integrator loop gain could be fixed to 0.8 even if the LGS flux is varying between 20 and 500 photons/subaperture/frame without loosing a lot of quality, as shown in Figure 6.

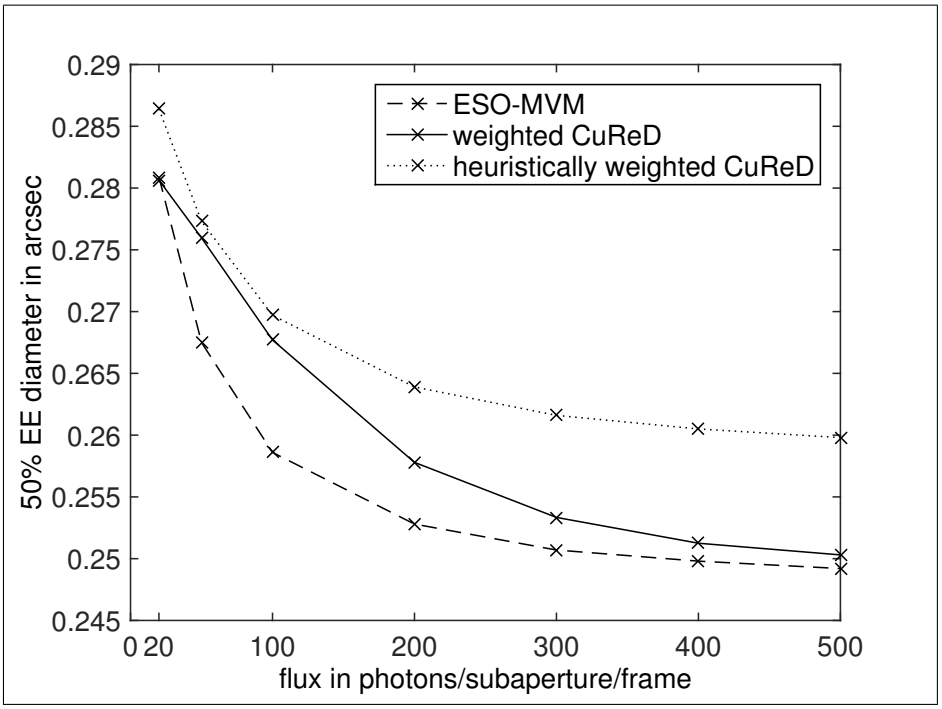

Figure 5: Simulation results comparing our algorithm to the existing ESO-MVM and heuristically weighted CuReD.

We want to emphasize again, that our approach does not require to tune any parameter besides α and the integrator loop gain. Moreover, the covariance matrices depend on the photon flux.

5 Remarks

Our approach of weighting the measurements can handle different flux from each GS, if this is incorporated in the corresponding covariance matrix. We did not perform tests for such a setting, as usually all LGS have the same flux.

We remark, that we did not consider possible overlapping of the elongated spots to neighboring subapertures. There might be some improvement possible into this direction.

For this paper, we considered perfectly aligned WFS only. In the non aligned case, which will cause misregistration effects between different WFS pupils, some more computations have to be done, if one wants to perform a weighting on measurements. WFS could be shifted/rotated with respect to each other, i.e., the subapertures do not lie on the same place. Such shifts and/or rotations need to be modeled in the weighting process. Rotations should be straight forward whereas shifts of two WFS with respect to each other might be a bit tricky to handle, even if they are small as one has to shift the measurements which are

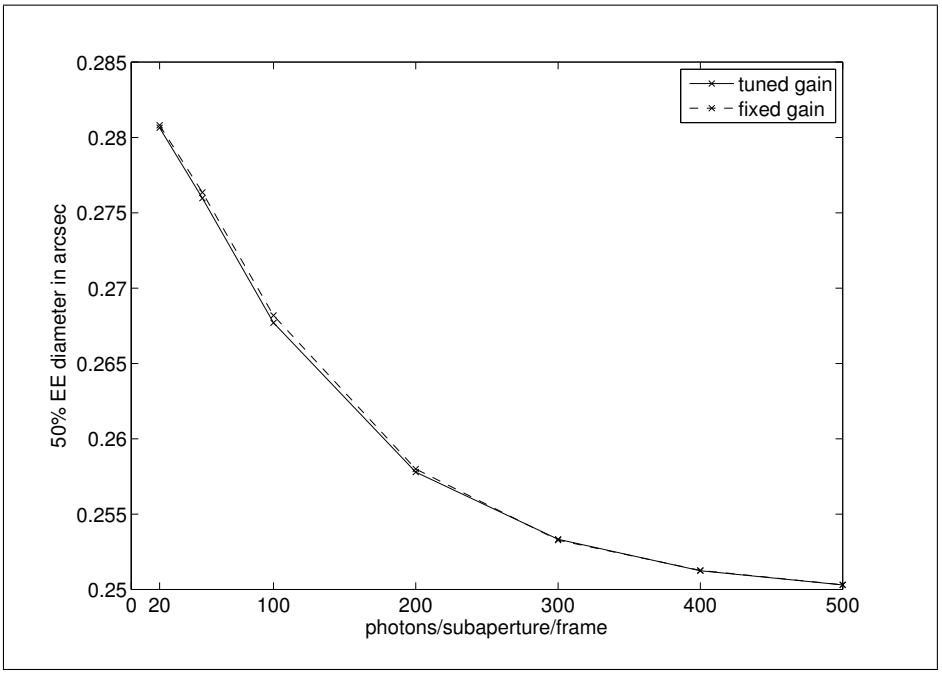

Figure 6: Simulation results comparing the tuned integrator loop gain and integrator loop gain fixed to 0.8.

derivatives. Misregistrations between WFS pupils and DM pupil just require a simple mapping.

Note that as quality criterion the PSF for the 50% EE evaluation is in center direction only. Evaluating the PSF in other directions requires some more work, but for our setting no other comparable results were available.

6 Conclusion

In this paper, we presented a fast and stable method to handle spot elongation effects in a GLAO system having LGS and NGS, making use of the fast wavefront reconstruction by CuReD. We want to emphasize that the computational costs for weighting the measurements are linear in the number of active subapertures and can be parallelized. Furthermore, the method is stable with respect to changes of the LGS photon flux and also with respect to changes in the integrator loop gain. Compared to the MVM results provided by the ESO, our method achieves comparable quality while maintaining clear advantage in the speed. The quality of our method also dominates the existing methods using CuReD without compromising the speed.

The main benefit of the preprocessing method is that it does not need any parameter choices and the integrator loop gain can be chosen very high for all flux levels. It is even possible to set the same integrator loop gain for all flux levels between 20 and 500 photons/subaperture/frame without losing much

quality. The combination of NGS and LGS measurements can be performed directly on measurements taking spot elongation into account. We emphasize that the regularization parameter α only requires small adjustments, if any at all as for all testcases $\alpha = 0.5$ gives satisfying results. The only variable parameter that has to be known is the photon flux in order to take the correct covariance matrix for each WFS.

In this work we studied the setting with perfectly aligned WFSs. For not aligned WFS some adjustments of the method are required and are presented in a forthcoming paper.

Funding Information

Funding. The work of RW and RR was funded by Hochschulraumstrukturmittel provided by the Austrian Ministry of Research (bmwfw). TH was supported by the Academy of Finland via the grant 275177.

Acknowledgments

RW wants to thank I. Shatokhina from JKU Linz, Austria, and M. Le Louarn from ESO for stimulating discussions and suggestions.

References

[1] AAO-Team. An introduction to MOST, the AAO-team internal AO-simulation tool. Technical Report E-TRE-AAO-528-0024, Austrian In-Kind Contribution - AO, 2012.

[2] Clémentine Béchet, Michel Tallon, Isabelle Tallon-Bosc, Éric Thiébaut, Miska Le Louarn, and Richard M. Clare. Optimal reconstruction for closed-loop ground-layer adaptive optics with elongated spots. *J. Opt. Soc. Am. A*, 27(11):A1–A8, Nov 2010.

[3] C. Béchet, M. Le Louarn, R. Clare, M. Tallon, M., I. Tallon-Bosc, and É. Thiébaut. Closed-loop ground layer adaptive optics simulations with elongated spots : impact of modeling noise correlations. *1st AO4ELT conference - Adaptive Optics for Extremely Large Telescopes*, page 03004, 2010.

[4] R. Clare, M. Le Louarn, C. Bechet, and E. Fedrigo. Use cases reference results. Technical Report E-TRE-ESO-520-1024 Issue 1, ESO, 2011.

[5] Richard M. Clare, Miska Le Louarn, and Clementine Béchet. Optimal noise-weighted reconstruction with elongated shack–hartmann wavefront sensor images for laser tomography adaptive optics. *Appl. Opt.*, 49(31):G27–G36, Nov 2010.

[6] Richard M. Clare, Miska Le Louarn, and Clementine Béchet. Laser guide star wavefront sensing for ground-layer adaptive optics on extremely large telescopes. *Appl. Opt.*, 50(4):473–483, Feb 2011.

[7] B. Ellerbroek, L. Gilles, and C.R. Vogel. A computationally efficient wavefront reconstructor for simulation or multi-conjugate adaptive optics on giant telescopes. *Proc. SPIE*, 4839, 2002.

[8] T. Fusco, J.-M. Conan, G. Rousset, L.M. Mugnier, and V. Michau. Optimal wave-front reconstruction strategies for multi conjugate adaptive optics. *J. Opt. Soc. Am. A*, 18(10):2527–2538, 2001.

[9] L. Gilles. Closed-loop stability and performance analysis of least squares and minimum-variance control algorithms for multiconjugate adaptive optics. *Appl. Opt.*, 44:993–1002, 2005.

[10] L. Gilles, B.L. Ellebroek, and C.R. Vogel. Preconditioned conjugate gradient wave-front reconstructors for multiconjugate adaptive optics. *Applied Optics*, 42(26):5233–5250, 2003.

[11] L. Gilles, B. Ellerbroek, and C.R. Vogel. Layer-oriented multigrid wavefront reconstruction algorithms for multi-conjugate adaptive optics. *Proc. SPIE*, 4839, 2002.

[12] T. Helin and M. Yudytskiy. Wavelet methods in multi-conjugate adaptive optics. *Inverse Problems*, 29(8):085003, 2013.

[13] J. Kaipio and E. Somersalo. *Statistical and Computational Inverse Problems*, volume 160 of *Applied Mathematical Sciences*. Springer Science+Business Media, Inc, 2005.

[14] Miska Le Louarn, Christophe Verinaud, Visa Korkiakoski, Norbert Hubin, and Enrico Marchetti. Adaptive optics simulations for the European Extremely Large Telescope - art. no. 627234. In *Advances in Adaptive Optics II, Prs 1-3*, volume 6272, pages U1048–U1056, 2006.

[15] M. Le Louarn, C. Vérinaud, V. Korkiakoski, N. Hubin, and E. Marchetti. Adaptive optics simulations for the European Extremely Large Telescope. In *Proc. SPIE 6272, Advances in Adaptive Optics II*, 2006.

[16] R. Ramlau, D. Saxenhuber, and M. Yudytskiy. Iterative reconstruction methods in atmospheric tomography: FEWHA, Kaczmarz and Gradient-based algorithm. In *Proc. SPIE*, volume 9148, pages 91480Q–91480Q–15, 2014.

[17] M. Rosensteiner. Cumulative reconstructor: fast wavefront reconstruction algorithm for Extremely Large Telescopes. *J. Opt. Soc. Am. A*, 28(10):2132–2138, Oct 2011.

[18] M. Rosensteiner. Solving the GLAO problem with the CuReD. Technical Report E-TRE-AAO-528-0009, Austrian In-Kind Contribution - AO, 2011.

[19] M. Rosensteiner. Wavefront reconstruction for extremely large telescopes via CuRe with domain decomposition. *J. Opt. Soc. Am. A*, 29(11):2328–2336, Nov 2012.

[20] M. Rosensteiner and R. Ramlau. Efficient iterative atmospheric tomography reconstruction from LGS and additional tip/tilt measurements. In *SPIE 8447, Adaptive Optics Systems III*, pages 84475S–84475S–6, 2012.

[21] M. Rosensteiner and R. Ramlau. The Kaczmarz algorithm for multi-conjugate adaptive optics with laser guide stars. *J. Opt. Soc. Am. A*, 30(8):1680–1686, 2013.

[22] Andrew M Stuart. Inverse problems: a Bayesian perspective. *Acta Numerica*, 19:451–559, 2010.

[23] Michel Tallon, Isabelle Tallon-Bosc, Clémentine Béchet, and Eric Thiébaut. Shack-hartmann wavefront reconstruction with elongated sodium laser guide stars: improvements with priors and noise correlations. volume 7015, page 70151N. SPIE, 2008.

[24] C.R. Vogel and Q. Yang. Fast optimal wavefront reconstruction for multi-conjugate adaptive optics using the Fourier domain preconditioned conjugate gradient algorithm. *Optics Express*, 14(17), 2006.

[25] M. Yudytskiy. *Wavelet methods in adaptive optics*. PhD thesis, Johannes Kepler University Linz, 2014.

[26] M. Yudytskiy, T. Helin, and R. Ramlau. Finite element-wavelet hybrid algorithm for atmospheric tomography. *J. Opt. Soc. Am. A*, 31(3):550–560, Mar 2014.

[27] M. Zhariy, A. Neubauer, M. Rosensteiner, and R. Ramlau. Cumulative wavefront reconstructor for the Shack-Hartman sensor. *Inverse Problems and Imaging*, 5(4):893–913, Nov 2011.